# Spectroscopic properties and radiative lifetimes of SiTe: A high-level multireference configuration interaction investigation*

Li Rui(李 瑞)[a)†], Zhang Xiao-Mei(张晓美)[b)], Jin Ming-Xing(金明星)[b)‡], Xu Hai-Feng(徐海峰)[b)], and Yan Bing(闫 冰)[b)]

[a)] *Department of Physics, College of Science, Qiqihar University, Qiqihar* 161006, *China*
[b)] *Institute of Atomic and Molecular Physics, Jilin University, Changchun* 130012, *China*

(Received 17 December 2013; revised manuscript received 15 January 2014; published online 25 March 2014)

The 18 Λ–S states correlated to the lowest dissociation limit of SiTe were calculated by using a high-level multireference configuration interaction (MRCI) method, including scalar relativistic and spin–orbit coupling effects. Based on the calculated potential energy curves, the spectroscopic constants of bound states were determined, which are well consistent with previous experimental results. The spin–orbit matrix elements between the Λ–S states were computed, which lead to an in-depth understanding of perturbations on the electronic state $a^3\Pi$. Finally, the transition dipole moments of allowed transitions $A^1\Pi$–$X^1\Sigma^+$, $E^1\Sigma^+$–$X^1\Sigma^+$, $a^3\Pi$–$d^3\Delta$, $a^3\Pi$–$a'^3\Sigma^+$, $a^3\Pi$–$e^3\Sigma^-$, and the radiative lifetimes of $A^1\Pi$, $E^1\Sigma^+$, and $a^3\Pi$ were evaluated.

**Keywords:** silicon monotelluride (SiTe), spectroscopic constants, transition dipole moment, radiative lifetime

**PACS:** 31.50.Df, 31.15.aj, 31.15.ag **DOI:** 10.1088/1674-1056/23/5/053101

## 1. Introduction

Silicon chalcogenides, which play important roles in a variety of research fields and they have received considerable attention for a long time. Among these molecules, the spectroscopic properties of SiO/SiS[1–5] have been extensively studied because of their importance in circumstellar chemistry. In contrast to the lighter species SiO/SiS, fewer investigations have been performed on heavier species SiTe. For SiTe, the ultraviolet $A^1\Pi$–$X^1\Sigma^+$ absorption band system was initially recorded by Barrow *et al.* in the range of 3200–3900 Å.[6] Subsequently, a series of spectroscopic studies have been carried out to study the excited states of SiTe. The singlet excited states $A^1\Pi$ and $E^1\Sigma^+$ have been measured by quite a few groups during the past few decades. The ultraviolet $A^1\Pi$–$X^1\Sigma^+$band system was observed by different experimental techniques,[7–10] and the spectroscopic constants of $A^1\Pi$ and $X^1\Sigma^+$ were derived. Another E–$X^1\Sigma^+$ transition of SiTe[7] was observed in the ultraviolet region at high temperature (800–1000 °C), whereas the study incorrectly assigned the E state to $^3\Sigma^+$ symmetry. Later, Lakshminarayana *et al.* demonstrated that the E state is of $^1\Sigma^+$ symmetry, and they also corrected the previous vibrational constants of the $E^1\Sigma^+$. For the ground state $X^1\Sigma^+$, the dissociation energy was determined to be 4.64 eV[11,12] through the thermodynamic method. Recently, the spectroscopic parameters of bound states were obtained by employing configuration interaction calculations[13] and an effective isotopic error compensation (IEC) approach.[14]

In recent years, with the rapid development of high-resolution spectroscopic techniques and computational methods, some deep insights into the electronic structures for the molecules that contain heavier atoms have been achieved. New band system and more accurate spectroscopic constants of the heavy-element molecules have been continually reported in the literatures.[15,16] However, there is still lack of a complete quantitative picture of the perturbations between low-lying excited states of SiTe, which have obvious influence on the spectroscopic and dynamic characters of electronic states. Particularly, the evident spin–orbit coupling (SOC) of heavy element Te leads to complicated interactions of electronic states for SiTe.

In this work, we performed the relativistic configuration interaction study on the excited states of SiTe. The potential energy curves (PECs) of all 18 Λ–S states correlated to the lowest dissociation limit (Si($^3$P)+Te($^3$P)) were computed. The SOC of these Λ–S states and the spin-allowed transition dipole moments (TDMs) were also obtained utilizing high-level *ab initio* calculation approaches. On the basis of the calculated PECs, the spectroscopic constants for the bound states of SiTe were deduced by the solution of nuclear Schrödinger equation. Finally, the radiative lifetimes of the low-lying vibrational states of $A'^1\Sigma^+$, $A^1\Pi$, and $a^3\Pi$ were obtained.

*Project supported by the National Natural Science Foundation of China (Grant Nos. 11034003, 11074095, and 11274140), the Natural Science Foundation of Heilongjiang Province, China (Grant No. F201335), and the Scientific and Technological Research Foundation of Qiqihar, China (Grant No. GYGG-201209-1).

†Corresponding author. E-mail: lirei01@163.com
‡Corresponding author. E-mail: mxjin@jlu.edu.cn

© 2014 Chinese Physical Society and IOP Publishing Ltd 

## 2. Methods and computational details

In the present work, the *ab initio* calculations were performed by using MOLPRO 2010[17] program. The symmetry point group of SiTe is $C_{\infty v}$. However, owing to the limitation of the MOLPRO program, all the calculations were carried out in the $C_{2v}$ subgroup of $C_{\infty v}$ point group. The relationships between the irreducible representations of $C_{2v}$ and $C_{\infty v}$ groups are $\Sigma^+ = A_1$, $\Pi = B_1 + B_2$, $\Delta = A_1 + A_2$, and $\Sigma^- = A_2$. In the subsequent calculations, we used the relativistic contracted atomic natural orbital basis sets (ANO-RCC)[18] to describe the Si and Te atoms. At a series of given bond lengths between 2.0 and 5.0 Å, the 18 lowest Λ–S states of SiTe were computed with state-averaged complete active space self-consistent field (CASSCF) method[19,20] using the Hartree–Fock molecular orbitals (MOs) as the starting orbitals. In the CASSCF calculations, the active space of SiTe includes Si 3p and Te 5s5p6s6p$_x$6p$_y$ orbitals. Furthermore, by employing the CASSCF energies as reference values, the energies of the 18 Λ–S states were calculated by the internally contracted multireference configuration interaction approach[21,22] with the Davison correction (MRCI+Q).[23] For MRCI+Q calculations, the $3s^2 3p^2$ electrons of Si and the $5s^2 5p^4$ electrons of Te were correlated, while the remaining inner electrons were frozen and not correlated.

In the above calculations, the scalar relativistic correction was taken into account via the third-order Douglas–Kroll (DK3)[24,25] approximation with ANO-RCC basis sets. The SOC effect was evaluated with state-interacting method using the Breit–Pauli operator.[26] In the SOC calculations, the spin–orbit integrals between the low-lying Λ–S states of SiTe were obtained from MRCI wave functions.

Based on the calculated PECs, the spectroscopic constants, including adiabatic transition energies ($T_e$), harmonic vibrational frequencies ($\omega_e$), anharmonic constants ($\omega_e x_e$), rotational constants ($B_e$), and equilibrium bond lengths ($R_e$), were evaluated by the numerical solution of nuclear Schrödinger equations using Le Roy's LEVEL procedure.[27]

## 3. Results and discussion

### 3.1. PECs and spectroscopic parameters of the low-lying Λ–S states

The 18 Λ–S states correlated to the lowest dissociation limit Si($^3$P)+Te($^3$P) for SiTe were computed at the ANO-RCC/MRCI+Q level of theory. The corresponding PECs are plotted in Fig. 1. These PECs are positioned in energy relative to the minimum energy point of the ground state $X^1\Sigma^+$ of SiTe. Each PEC is constructed with 38 discrete energy points at a series of given bond lengths from 2.0 Å to 5.0 Å. The 18 Λ–S states have three sets of spin multiplicity, 6 singlet Λ–S states ($X^1\Sigma^+$, $1^1\Sigma^-$, $1^1\Delta$, $A^1\Pi$, $E^1\Sigma^+$, and $2^1\Pi$), 6 triplet Λ–S states, ($a'^3\Sigma^+$, $d^3\Delta$, $e^3\Sigma^-$, $a^3\Pi$, $2^3\Pi$, and $2^3\Sigma^+$), and 6 quintet states ($1^5\Sigma^+$, $1^5\Pi$, $2^5\Sigma^+$, $2^5\Pi$, $1^5\Sigma^-$, and $1^5\Delta$). As illustrated in Fig. 1, apart from three high-lying excited states, $2^1\Pi$, $2^3\Pi$, and $2^3\Sigma^+$, the other singlet/triplet electronic states are essentially bound states and hold deep potential wells. For quintet states, except for the weakly bounded states ($1^5\Sigma^+$ and $1^5\Pi$), all the other four quintet Λ–S states are typically repulsive. The fitted spectroscopic constants of bound Λ–S states are listed in Table 1. In order to illuminate the influence resulting from scalar relativistic effect, the spectroscopic constants obtained from PECs excluding the scalar relativistic effect with the entirely uncontracted ANO-RCC basis set are also given in Table 1 for comparison. The leading electronic configuration of the low-lying Λ–S states at $R = 2.3$ and 3.0 Å are given in Table 2.

The ground state $X^1\Sigma^+$ is mainly derived from the closed-shell electronic configuration $16\sigma^2 17\sigma^2 7\pi^4$. In comparison to recent experimental results,[28] with inclusion of the scalar relativistic effect, the spectroscopic constants $\omega_e$, $\omega_e x_e$, $B_e$, and $R_e$ of $X^1\Sigma^+$ state are improved by 2.84, 0.8716, 0.0016 cm$^{-1}$, and 0.0132 Å, and our best calculated $\omega_e$, $\omega_e x_e$, and $B_e$ values of the state are only 3.88, 0.1084, and 0.0025 cm$^{-1}$ smaller, whereas the $R_e$ value is only 0.0203 Å larger. The dissociation energy is calculated to be 4.67 eV, which are in excellent agreement with previous experimental data of 4.64 eV.[11,12]

As shown in Fig. 1 and Table 1, the low-lying excited states ($1^1\Sigma^-$, $1^1\Delta$, $a^3\Pi$, $a'^3\Sigma^+$, $d^3\Delta$, and $e^3\Sigma^-$) exhibit a high density in the energy range of 16500–22000 cm$^{-1}$. Due to the large state density, spin–orbit and rotational couplings of these electronic states are expected to occur. Numerous interactions between these electronic states lead to the avoided crossings, which could make the band system of corresponding electronic states hard to be observed in experiments. The perturbations between these electronic states will be separately discussed in the next section. The $1^1\Sigma^-$, $1^1\Delta$, $a'^3\Sigma^+$, $d^3\Delta$, and $e^3\Sigma^-$ originate from the open-shell electronic configuration $16\sigma^2 17\sigma^2 7\pi^3 8\pi^1$, while $a^3\Pi$ comes from the open-shell

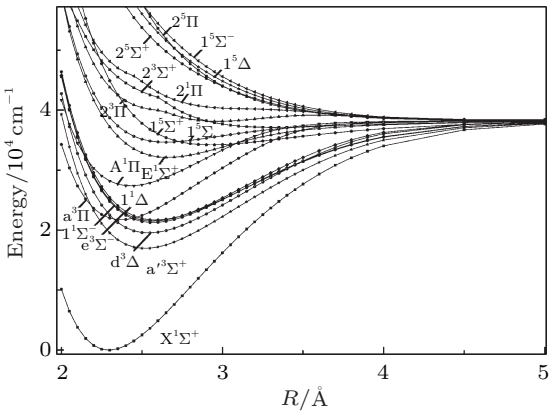



**Fig. 1.** Calculated MRCI+Q potential energy curves of the ground and low-lying excited states of SiTe molecule.

**Table 1.** Computed and experimental spectroscopic constants of SiTe.

| State | | $T_e$/cm$^{-1}$ | $\omega_e$/cm$^{-1}$ | $\omega_e x_e$/cm$^{-1}$ | $B_e$/cm$^{-1}$ | $R_e$/Å |
|---|---|---|---|---|---|---|
| $X^1\Sigma^+$ | This work[a)] | 0 | 476.83 | 1.2717 | 0.1396 | 2.2939 |
| | This work[b)] | 0 | 473.99 | 0.4001 | 0.1380 | 2.3071 |
| | Expt.[c)] | 0 | 481.2 | 1.30 | | |
| | Expt.[d)] | 0 | 481.04(9) | 1.288(20) | 0.14190(2) | |
| | Expt.[e)] | 0 | 480.656(15) | 1.3428(18) | 0.141661(4) | |
| | Expt.[f)] | 0 | 480.71(51) | 1.3801(20) | 0.142062548(3) | 2.273593049(22) |
| $a^3\Pi$ | This work[a)] | 21723 | 386.56 | 1.3516 | 0.1307 | 2.3700 |
| $a'^3\Sigma^+$ | This work[a)] | 16961 | 342.09 | 0.9399 | 0.1158 | 2.5187 |
| $d^3\Delta$ | This work[a)] | 19558 | 333.80 | 1.1270 | 0.1138 | 2.5400 |
| $e^3\Sigma^-$ | This work[a)] | 21503 | 318.72 | 1.1586 | 0.1114 | 2.5684 |
| $A^1\Pi$ | This work[a)] | 27374 | 344.30 | 1.7306 | 0.1245 | 2.4293 |
| | This work[b)] | 27222 | 339.30 | 1.2300 | 0.1231 | 2.4422 |
| | Expt.[c)] | 28661.8 | 338.6 | 1.70 | | |
| | Expt.[d)] | 28660.46(5) | 338.31(3) | 1.668 (7) | 0.12491(2) | |
| | Expt.[e)] | 28660.76(8) | 337.673(51) | 1.5917(118) | 0.124810(27) | |
| $1^1\Sigma^-$ | This work[a)] | 21264 | 317.34 | 1.1848 | 0.1113 | 2.5694 |
| $1^1\Delta$ | This work[a)] | 21771 | 310.19 | 1.2053 | 0.1101 | 2.5834 |
| $1^5\Pi$ | This work[a)] | 34654 | 226.70 | 3.5650 | 0.1049 | 2.6454 |
| $E^1\Sigma^+$ | This work[a)] | 32130 | 264.67 | 1.7196 | 0.1039 | 2.6593 |
| | This work[b)] | 32128 | 273.81 | 2.1336 | 0.1035 | 2.6594 |
| | Expt.[c)] | 33991 | 242 | | | |
| | Expt.[g)] | 34000.31 | 229.86 | 1.190 | | |
| $2^3\Pi$ | This work[a)] | 38139 | 184.31 | 4.8895 | 0.0834 | 2.9673 |
| $1^5\Sigma^+$ | This work[a)] | 34213 | 171.59 | 1.8049 | 0.0855 | 2.9299 |

Note: For the experimental values, the inaccuracy of measurement is given in the bracket.
[a)] This work, with the scalar relativistic effect, [b)] this work, without the scalar relativistic effect, [c)] Ref. [29], [d)] Ref. [8], [e)] Ref. [10], [f)] Ref. [28], [g)] Ref. [9].

**Table 2.** Leading electronic configuration of low-lying states of SiTe for $R = 2.3$ Å and 3.0 Å.

| State | $R = 2.3$ Å | $R = 3.0$ Å |
|---|---|---|
| $X^1\Sigma^+$ | $16\sigma^2 17\sigma^2 7\pi^4$ (80%) | $16\sigma^2 17\sigma^2 7\pi^4$ (44%) |
| | | $16\sigma^2 17\sigma^2 7\pi^3 8\pi^1$ (37%) |
| $a^3\Pi$ | $16\sigma^2 17\sigma^1 7\pi^4 8\pi^1$ (81%) | $16\sigma^2 17\sigma^1 7\pi^4 8\pi^1$ (64%) |
| | | $16\sigma^2 17\sigma^1 7\pi^4 8\pi^1$ (11%) |
| $a'^3\Sigma^+$ | $16\sigma^2 17\sigma^2 7\pi^3 8\pi^1$ (91%) | $16\sigma^2 17\sigma^2 7\pi^3 8\pi^1$ (82%) |
| $A^1\Pi$ | $16\sigma^2 17\sigma^1 7\pi^4 8\pi^1$ (90%) | $16\sigma^2 17\sigma^1 7\pi^4 8\pi^1$ (55%) |
| | | $16\sigma^2 17\sigma^1 7\pi^3 8\pi^2$ (19%) |
| $d^3\Delta$ | $16\sigma^2 17\sigma^2 7\pi^3 8\pi^1$ (92%) | $16\sigma^2 17\sigma^2 7\pi^3 8\pi^1$ (86%) |
| $e^3\Sigma^-$ | $16\sigma^2 17\sigma^2 7\pi^3 8\pi^1$ (91%) | $16\sigma^2 17\sigma^2 7\pi^3 8\pi^1$ (85%) |
| $1^1\Sigma^-$ | $16\sigma^2 17\sigma^2 7\pi^3 8\pi^1$ (91%) | $16\sigma^2 17\sigma^2 7\pi^3 8\pi^1$ (82%) |
| $1^1\Delta$ | $16\sigma^2 17\sigma^2 7\pi^3 8\pi^1$ (90%) | $16\sigma^2 17\sigma^2 7\pi^3 8\pi^1$ (82%) |
| $E^1\Sigma^+$ | $16\sigma^2 17\sigma^2 7\pi^3 8\pi^1$ (58%) | $16\sigma^2 17\sigma^2 7\pi^2 8\pi^2$ (39%) |
| | $16\sigma^2 17\sigma^1 18\sigma^1 7\pi^4$ (13%) | $16\sigma^2 17\sigma^1 18\sigma^1 7\pi^4$ (17%) |
| | | $16\sigma^2 17\sigma^2 7\pi^3 8\pi^1$ (15%) |

electronic configuration $16\sigma^2 17\sigma^1 7\pi^4 8\pi^1$. The equilibrium distance ($R_e$) of $a^3\Pi$ is calculated to be 2.3700 Å, which is obviously shorter than those of $1^1\Sigma^-$, $1^1\Delta$, $a'^3\Sigma^+$, $d^3\Delta$, and $e^3\Sigma^-$ states (2.52–2.58 Å), indicating that $7\pi$ molecular orbital (MO) is somewhat more bonding than the $17\sigma$ MO in the SiTe.

The excited state $A^1\Pi$ is mainly characterized by open-shell electronic configuration $16\sigma^2 17\sigma^1 7\pi^4 8\pi^1$, which is the same as that of $a^3\Pi$. According to the calculation results, the scalar relativistic effect gives corrections of 152, 5, and 0.5006 cm$^{-1}$ on the $T_e$, $\omega_e$, and $\omega_e x_e$ values of $A^1\Pi$ When taking into account the scalar relativistic effect, the $T_e$, $\omega_e$, $\omega_e x_e$, and $B_e$ values of $A^1\Pi$ are calculated to be 27374, 344.30, 1.7306, and 0.1245 cm$^{-1}$, respectively, which match excellently well with the latest experimental values of 28660.76, 337.673, 1.5917, and 0.124810 cm$^{-1}$. Our calculations predict the $R_e$ of $A^1\Pi$ to be 2.4293 Å.

Above the $A^1\Pi$ state, $E^1\Sigma^+$ state is mainly described by open-shell electronic configuration $16\sigma^2 17\sigma^2 7\pi^3 8\pi^1$ Comparing with the previous experimental results, with including the scalar relativistic effect, the $T_e$, $\omega_e$, and $\omega_e x_e$ of $E^1\Sigma^+$ are improved by 2, 9.14, and 0.4140 cm$^{-1}$, and our best computed $T_e$, $\omega_e$, and $\omega_e x_e$ values of $E^1\Sigma^+$ differ by less than 1870, 34.81, and 0.5296 cm$^{-1}$, respectively. Nevertheless, the relatively large deviation for the calculated $T_e$ of $E^1\Sigma^+$ is found, which may be caused by the omitting of core-valence correlation effect for $4d^{10}$ electrons of Te atom. The $B_e$ and $R_e$ values of $E^1\Sigma^+$ have not been determined in previous experimental studies, which are predicted to be 0.1039 cm$^{-1}$ and 2.6593 Å in our work.

The dipole moments of the 18 Λ–S states were computed at the MRCI level of theory. The dipole moment curves of

those Λ–S states are shown in Fig. 2. At equilibrium bond length of SiTe, the dipole moment of the ground state $X^1\Sigma^+$ is −0.23 a.u., indicating the $Si^+Te^-$ polarity for the molecule. As shown in Fig. 2, the dipole moments of quintet states are positive over the internuclear distance, while the changes of polarity exist in that of singlet and triplet states. At the large separation, the dipole moment values of these states are all close to zero, reflecting that the dissociation products are neutral atoms.

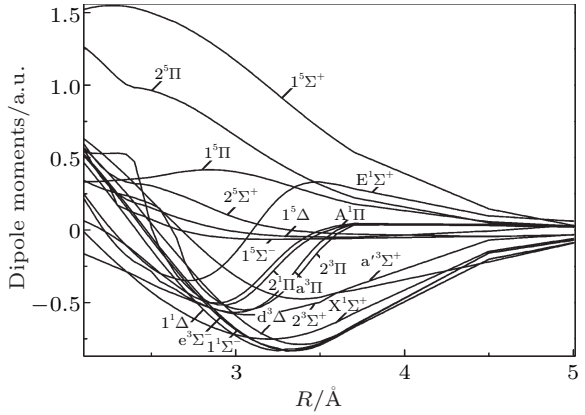



**Fig. 2.** Dipole moment functions for the 18 Λ–S states of SiTe.

### 3.2. Analysis of spin–orbit perturbations in $a^3\Pi$ and $A^1\Pi$ states

As indicated in Fig. 1 and Table 1, there is a high state density of SiTe molecule in the energy region of 16500–27400 $cm^{-1}$, which can give rise to complicated interactions among these electronic states. For clarity, an amplified view of PECs of the states in the crossing region is displayed in Fig. 3, together with the vibrational levels $v' = 14$ of $A^1\Pi$ state and $v' = 0$–5 of the $a^3\Pi$ state. As shown in Fig. 3, the $A^1\Pi$ crosses with $1^1\Sigma^-$, $e^3\Sigma^-$, and $1^1\Delta$ states at $R = 2.15$ Å, and $a^3\Pi$ crosses with $a'^3\Sigma^+$, $d^3\Delta$, $1^1\Sigma^-$, $e^3\Sigma^-$, and $1^1\Delta$ states at bond length between 2.2–2.5 Å. Due to all the seven bound states correlated to the lowest dissociation limit, the interactions between the states could only lead to the perturbations rather than predissociation. When the SOC effect is taken into consideration, avoided crossings occur at the crossing points of these states with the same Ω component, and have great influence on the line intensity, position, and shape of the spectrum. The $A^1\Pi$ state crosses with $1^1\Sigma^-$, $e^3\Sigma^-$, and $1^1\Delta$ states at $R = 2.15$ Å, around the $v' = 14$ vibrational level of the $A^1\Pi$ state. Our calculated results demonstrate that $v' = 0$–13 vibrational levels of $A^1\Pi$ are unperturbed by the adjacent states, which has been verified in previous experimental study[9] by Lakshminarayana *et al.* They have only observed the $v' = 0$–12 vibrational levels of the $A^1\Pi$ state. The $a^3\Pi$ crosses with $a'^3\Sigma^+$, $d^3\Delta$, $1^1\Sigma^-$, $e^3\Sigma^-$, and $1^1\Delta$ states at $R = 2.19$, 2.31, 2.44, 2.46, and 2.48 Å, near $v' = 5$, 0, 0, 0, 1 vibrational levels of the $a^3\Pi$ state. Hence, the $v' = 0$–5 vibrational states of $a^3\Pi$ state may be perturbed by interactions with the corresponding vibrational states of other closing electronic states.

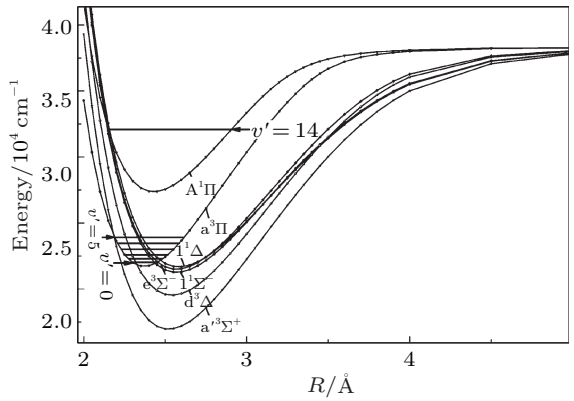



**Fig. 3.** An amplified view of the crossing region of the potential energy curves for the electronic states $a^3\Pi$ and $A^1\Pi$ together with identify of vibrational levels of those states around the crossing point.

In order to further illuminate the perturbations in $A^1\Pi$ and $a^3\Pi$ states, the spin–orbit matrix elements of $A^1\Pi$ and $a^3\Pi$ with the other states were computed in our work. Figure 4 displays the absolute values of spin–orbit matrix elements including $A^1\Pi$ and $a^3\Pi$ states as a function of the bond length. The definitions of the schematic terms of spin–orbit elements appeared in Fig. 4 are given in Table 3. The spin–orbit matrix elements between $a^3\Pi$ and $a'^3\Sigma^+$, $d^3\Delta$, $e^3\Sigma^-$, $1^1\Delta$ or $1^1\Sigma^-$ exhibit similar behavior, which first gradually increase as the

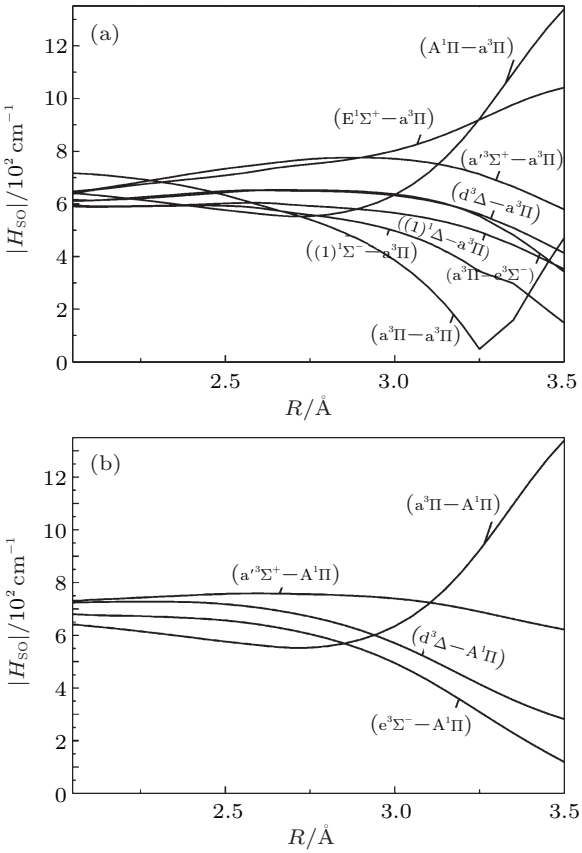



**Fig. 4.** Evolution of the absolute values of spin–orbit matrix elements including the $a^3\Pi$ and $A^1\Pi$ states along the bond length.

**Table 3.** Spin–orbit matrix elements between two interacting electronic states in the curves crossing region.

| Spin–orbit matrix elements |
|---|
| $i\langle a^3\Pi_x,\ m_s=1\|L_zS_z\|a^3\Pi_y,\ m_s=1\rangle = (a^3\Pi–a^3\Pi)$ |
| $\langle(1)^3\Sigma^+,\ m_s=0\|L_yS_y\|a^3\Pi_x,\ m_s=1\rangle = ((1)^3\Sigma^+–a^3\Pi)$ |
| $\langle(1)^3\Delta_x,\ m_s=0\|L_yS_y\|a^3\Pi_x,\ m_s=1\rangle = ((1)^3\Delta–a^3\Pi)$ |
| $\langle(1)^1\Delta_x,\ m_s=0\|L_yS_y\|a^3\Pi_x,\ m_s=1\rangle = ((1)^1\Delta–a^3\Pi)$ |
| $i\langle(1)^1\Sigma^-,\ m_s=0\|L_xS_x\|a^3\Pi_x,\ m_s=1\rangle = ((1)^1\Sigma^–a^3\Pi)$ |
| $i\langle a^3\Pi_x,\ m_s=0\|L_xS_x\|(1)^3\Sigma^-,\ m_s=1\rangle = (a^3\Pi\text{-}(1)^3\Sigma^-)$ |
| $\langle E^1\Sigma^+,\ m_s=0\|L_yS_y\|a^3\Pi_x,\ m_s=1\rangle = (E^1\Sigma^+–a^3\Pi)$ |
| $\langle A^1\Pi_x,\ m_s=0\|L_yS_y\|a^3\Pi_y,\ m_s=0\rangle = (A^1\Pi–a^3\Pi)$ |
| $\langle A^1\Pi_x,\ m_s=0\|L_yS_y\|(1)^3\Sigma^+,\ m_s=1\rangle = (A^1\Pi\text{-}(1)^3\Sigma^+)$ |
| $i\langle A^1\Pi_x,\ m_s=0\|L_xS_x\|(1)^3\Sigma^-,\ m_s=1\rangle = (A^1\Pi–(1)^3\Sigma^-)$ |
| $\langle A^1\Pi_x,\ m_s=0\|L_xS_x\|(1)^3\Delta_x,\ m_s=1\rangle = (A^1\Pi–(1)^3\Delta)$ |

Note: The right-hand parts are the schematic terms in Fig. 4, and the symbol i in the front of angular brackets indicates the imaginary part of spin–orbit matrix elements.

Si–Te bond length increases and then decrease sharply at large bond length region. However, the other spin–orbit matrix elements ($a^3\Pi$–$a^3\Pi$), ($a^3\Pi$–$A'^1\Sigma^+$), and ($A^1\Pi$–$a^3\Pi$) have obviously different variation trends. This phenomenon could come down to the same electronic configuration of the $a'^3\Sigma^+$, $d^3\Delta$, $e^3\Sigma^-$, $1^1\Delta$, and $1^1\Sigma^-$ states, which is mainly characterized by $16\sigma^2 17\sigma^2 7\pi^3 8\pi^1$ at both $R = 2.3$ Å and $R = 3.0$ Å. In addition, the $A^1\Pi$ and $a^3\Pi$ states mainly originate from the same electronic configuration $16\sigma^2 17\sigma^1 7\pi^4 8\pi^1$ at both $R = 2.3$ and 3.0 Å. Hence, the changing trends of the spin–orbit matrix curves including the $A^1\Pi$ state are similar to those including the $a^3\Pi$ state, despite that the maximum of the elements are at different $R$ values. At the crossing points, the absolute values of spin–orbit integral of $a^3\Pi$–$a'^3\Sigma^+$, $a^3\Pi$–$d^3\Delta$, $a^3\Pi$–$e^3\Sigma^-$, $a^3\Pi$–$1^1\Delta$, and $a^3\Pi$–$1^1\Sigma^-$ are 668, 629, 640, 599, and 592 $cm^{-1}$, respectively, which are large enough to perturb the $v' = 0$–5 vibrational states of $a^3\Pi$. It is therefore hard to observe the $a^3\Pi$–$X^1\Sigma^+$ band-system in experiment.

### 3.3. Radiative lifetimes of low-lying electronic states

The radiative lifetime of vibrational state $v'$ for an electronic state is defined as

$$\tau = \left(\sum_{v''} A_{v'v''}\right)^{-1}. \quad (1)$$

The Einstein coefficient $A_{v'v''}$ for spontaneous emission between vibrational levels $v'$ and $v''$ is obtained as

$$A_{v'v''} = 2.026 \times 10^{-6} \tilde{\upsilon}^3 \mathrm{TDM}^2 q_{v'v''}, \quad (2)$$

where $\tilde{\upsilon}$ is the transition energy in unit of $cm^{-1}$, TDM is the averaged electronic transition dipole moment in atomic unit, $q_{v'v''}$ is the Franck–Condon factor (FCF) between vibrational levels $v'$ and $v''$, and $\tau$ is in unit of second.

The transition dipole moments (TDMs) of spin-allowed transition $A^1\Pi$–$X^1\Sigma^+$, $E^1\Sigma^+$–$X^1\Sigma^+$, $a^3\Pi$–$d^3\Delta$, $a^3\Pi$–$a'^3\Sigma^+$, and $a^3\Pi$–$e^3\Sigma^-$ were calculated from MRCI wave functions. The evolution of absolute values for the TDMs along the bond length is plotted in Fig. 5. The TDM of $E^1\Sigma^+$–$X^1\Sigma^+$ transition is evidently larger than that of the remaining four transitions. It could also be found from Fig. 5 that the TDMs of $A^1\Pi$–$X^1\Sigma^+$, $E^1\Sigma^+$–$X^1\Sigma^+$, $a^3\Pi$–$d^3\Delta$, and $a^3\Pi$–$e^3\Sigma^-$ decrease gradually with the increase in bond length, while the TDM of $a^3\Pi$–$a'^3\Sigma^+$ decrease smoothly in bond length range of 2.1–2.65 Å and increase gradually when $R > 2.65$ Å. On the basis of our calculated TDMs, PECs, FCFs, and vibrational energy levels, the radiative lifetimes of the three lowest vibrational states of $A^1\Pi$, $E^1\Sigma^+$, and $a^3\Pi$ were evaluated, which are listed in Table 4. The evaluated radiative lifetimes are in the order of 10 ns and 100 ns for singlet states $A^1\Pi$ and $E^1\Sigma^+$, while being in the order of 100 μs for triplet state $a^3\Pi$.

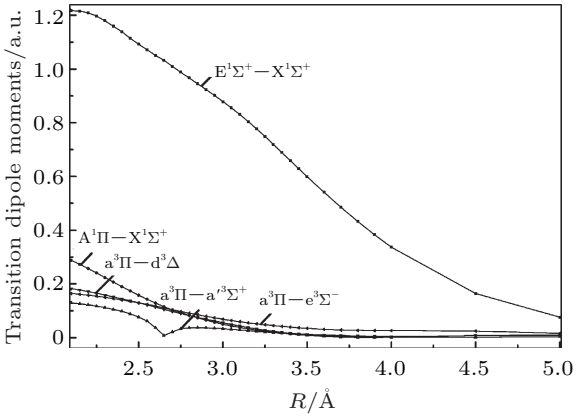



**Fig. 5.** Absolute values of the spin-allowed transition dipole moments as a function of bond length for SiTe.

**Table 4.** Radiative lifetimes (in ns) of the low-lying vibrational states of $E^1\Sigma^+$, $A^1\Pi$, and $a^3\Pi$.

| $v'$ | Radiative lifetimes | | | |
|---|---|---|---|---|
| | $\tau_{E-X}$ | $\tau_{A-X}$ | $\tau_{a-a'}$ | $\tau_{a-d}$ |
| 0 | 28 | 854 | $7.27 \times 10^5$ | $3.91 \times 10^5$ |
| 1 | 28 | 866 | $5.90 \times 10^5$ | $3.17 \times 10^5$ |
| 2 | 28 | 879 | $4.98 \times 10^5$ | $2.67 \times 10^5$ |
| 3 | 29 | 891 | $4.33 \times 10^5$ | $2.33 \times 10^5$ |

Note: E, A, a, a′, and d represent $E^1\Sigma^+$, $A^1\Pi$, $a^3\Pi$, $a'^3\Sigma^+$, and $d^3\Delta$ states, respectively.

## 4. Conclusions

In this work, we carried out MRCI+Q investigation on the 18 Λ–S states associated with the lowest dissociation limit ($Si(^3P)$+$Te(^3P)$) of SiTe. The scalar relativistic effect was treated by the third-order Douglas–Kroll (DK3) approximation. The spin–orbit coupling effect of the Λ–S states was taken into account via state-interacting method with the full Breit–Pauli operator. Based on the PECs of the Λ–S states, the spectroscopic constants of the bound states were determined and in good accord with previous experimental studies. With the aid of the spin–orbit matrix elements involving $a^3\Pi$, the perturbations on the vibrational states of $a^3\Pi$ are interpreted

in detail. The TDMs of spin-allowed transitions $A^1\Pi$–$X^1\Sigma^+$, $E^1\Sigma^+$–$X^1\Sigma^+$, $a^3\Pi$–$d^3\Delta$, $a^3\Pi$–$a'^3\Sigma^+$, and $a^3\Pi$–$e^3\Sigma^-$ were evaluated with the MRCI wave functions. Finally, the radiative lifetimes of the three lowest vibrational states of $A^1\Pi$, $E^1\Sigma^+$, and $a^3\Pi$ were obtained.

## References


[1] Campbell J M, Klapstein D, Dulick M, Bernath P F and Wallace L 1995 *Astrophys. J. Supp. Ser.* **101** 237

[2] Müller H S P, McCarthy M C, Bizzocchi L, Gupta H, Esser S, Lichau H, Caris M, Lewen F, Hahn J, Degli Esposti C, Schlemmer S and Thaddeus P 2007 *Phys. Chem. Chem. Phys.* **9** 1579

[3] Chattopadhyaya S, Chattopadhyay A and Das K K 2003 *J. Phys. Chem. A* **107** 148

[4] Xu G L, Lü W J, Liu Y F, Zhu Z L, Zhang X Z and Sun J F 2008 *Chin. Phys. B* **17** 4481

[5] Xu G L, Liu X F, Xie H X, Zhang X Z and Liu Y F 2011 *Chin. Phys. B* **20** 013101

[6] Barrow R F 1939 *Proc. Phys. Soc.* **51** 267

[7] Vago E E and Barrow R F 1946 *Proc. Phys. Soc.* **58** 538

[8] Bosser G and Lebreton J 1983 *J. Phys. B* **16** 39

[9] Lakshminarayana G and Gopal S 1990 *Pramana* **35** 519

[10] Gopal S, Singh M and Lakshminarayana G 1992 *Can. J. Phys.* **70** 291

[11] Exsteen G, Drowart J, Vander Auwera-Mahieu A and Callaerts R 1967 *J. Phys. Chem.* **71** 4130

[12] Ohare P A G 1993 *J. Phys. Chem. Ref. Data* **22** 1455

[13] Chattopadhyaya S, Pramanik A, Banerjee A and Das K K 2006 *J. Phys. Chem. A* **110** 12303

[14] Hou S, Long M, Zheng R and Sun W 2010 *Mol. Phys.* **108** 1491

[15] Alizadeh D, Jamshidi Z and Shayesteh A 2013 *Phys. Chem. Chem. Phys.* **15** 18678

[16] Li R, Wei C, Sun Q, Sun E, Jin M, Xu H and Yan B 2014 *J. Quant. Spectrosc. Radiat. Tran.* **133** 271

[17] Werner H J, Knowles P J, Knizia G, *et al.* 2010 *MOLPRO: a Package of ab initio* Programs

[18] Roos B O, Lindh R, Malmqvist P Å, Veryazov V and Widmark P O 2004 *J. Phys. Chem. A* **108** 2851

[19] Knowles P J and Werner H J 1985 *Chem. Phys. Lett.* **115** 259

[20] Werner H and Knowles P J 1985 *J. Chem. Phys.* **82** 5053

[21] Knowles P J and Werner H J 1988 *Chem. Phys. Lett.* **145** 514

[22] Werner H J and Knowles P J 1988 *J. Chem. Phys.* **89** 5803

[23] Langhoff S R and Davidson E R 1974 *Int. J. Quantum Chem.* **8** 61

[24] Douglas M and Kroll N M 1974 *Ann. Phys.* **82** 89

[25] Hess B A 1986 *Phys. Rev. A* **33** 3742

[26] Berning A, Schweizer M, Werner H J, Knowles P J and Palmieri P 2000 *Mol. Phys.* **98** 1823

[27] Le Roy R J 2002 *LEVEL 7.5: a Computer Program for Solving the Radial Schrödinger Equation for Bound and Quasibound Levels*

[28] Giuliano B M, Bizzocchi L and Grabow J U 2008 *J. Mol. Spectrosc.* **251** 261

[29] Huber K P and Herzberg G 1979 *Molecular Spectra and Molecular Structure IV, Constants of Diatomic Molecules* (New York: Van Nostrand-Reinhold)